Kulkarni *et al.*
Journal of Engineering and Applied Science (2024) 71:30
https://doi.org/10.1186/s44147-024-00374-1

Journal of Engineering and Applied Science

RESEARCH Open Access

Optimizing nanoparticle attributes for enhanced anti-wear performance in nano-lubricants

Trishul Kulkarni[1*], Bhagwan Toksha[2] and Arun Autee[1]

*Correspondence:
trishulkulkarni@gmail.com

[1] Department of Mechanical Engineering, Maharashtra Institute of Technology, Aurangabad 431010, India
[2] Faculty of Physics, Maharashtra Institute of Technology, Aurangabad 431010, India

Abstract

This study delves into optimizing nanoparticle attributes to enhance the anti-wear performance of nano-lubricants, specifically exploring the influence of nanoparticle material hardness and concentration. Investigating the impact of contamination-induced abrasive wear in lubricants and the subsequent enhancement of anti-wear properties through nanoparticle integration into base oil, the research focuses on, $CaCO_3$, TiO_2, and Al_2O_3 materials representing varied hardness levels. Using ASTM D4172 standards, the study examines the wear resistance of base oil infused with these nanoparticles. Employing a response surface methodology model based on experimental data, the criticality of the interaction between nanoparticle material hardness and concentration in determining wear effects is revealed. Analysis through atomic force microscopy and energy dispersive spectrometry aids in comprehending alterations in wear mechanisms. The research highlights the nuanced relationship between nanoparticle material hardness and concentration in shaping wear behavior within lubricants. Softer materials, like $CaCO_3$, demand higher concentrations for comparable wear reduction as observed with lower concentrations of harder materials, such as Al_2O_3. Conversely, higher concentrations of harder materials can exacerbate wear, as confirmed by EDS analysis and surface topography studies. This study underscores the importance of nanoparticle material hardness and concentration interaction in determining the efficacy of nanoparticles as anti-wear agents in lubricants. It emphasizes the need to optimize both factors for enhanced anti-wear properties in nanoparticle-based nano-lubricants, offering insights crucial for their application in practical scenarios.

Keywords: Nano-lubricant, Abrasive wear, Hardness, ANOVA, Response Surface Methodology (RSM)

Introduction

Abrasive wear is the most prevalent form of wear in lubricated machinery. An opposing surface that is moving relative to the first gets sliced and damaged by particle contamination and roughened surfaces [1, 2]. There are two main categories of abrasive wear: two-body and three-body. In two-body abrasive wear, two moving surfaces rub against one another. In this type of system, the wear rate is affected by both the hardness of the wearing surface and the hardness ratio between the two surfaces. A straightforward

model for explaining sliding wear is the Archard wear equation, which is based on the asperity contact theory. It claims that the wear volume (V) is inversely associated with the hardness of the softer contacting surface (H) and directly proportional to the sliding distance (L) and the applied load (W).

$$V = kWL/3H \tag{1}$$

where the wear coefficient, or constant *k*, can be used to compare the wear resistance of various materials [3, 4].

When abrasive particles are trapped between two surfaces, they can move in relation to one another and even rotate while gliding, which allows the material to be removed from either surface. When abrasive particles get lodged between two opposing sliding or rolling surfaces, it results in closed-body abrasive wear under particulate-contaminated lubrication conditions. [5]. Xuan et al. experimentally studied the effect of the hardness of the sliding surface and abrasive particles on three-body abrasive wear under fluid film lubrication. Important factors that affect three-body abrasive wear are the hardness of the abrasive particles and the two metal surfaces. Three-body abrasive wear is inversely associated with the hardness ratio between the abrasive particle and the wearing surface. When the difference between the surface hardness and abrasive particle hardness is large, the harder particle indents the softer surface and cuts the other sliding surface [3].

On the contrary, it has been established that employing nanoparticles (NPs) as friction modifiers (FMs) and anti-wear additives in the base lubricant oil can significantly reduce friction and wear. With the addition of various micro- and nano-sized particles to the base lubricating oil, friction and wear between two rubbing surfaces are significantly reduced, and the load-carrying capacity is increased [6]. Carbon-based materials, metals, metal oxides, nano-composites, rare-earth elements, and sulfides are the various nanoparticle (NP) materials dispersed in various types of lubricating oils to formulate the nano-lubricants [7–10]. The purpose of NP additives in base oils is to improve the lubricants' resistance to wear and friction; either of these can be used as tribological performance indicators [11]. The material [12], size [13], and shape [14] of NPs are the three key parameters related to NPs that influence the tribological performance of nano-lubricants. The NP concentration in base oil also has an effect on tribological system performance [15]. In addition to these input characteristics, which are commonly discussed in the literature, base oil lubricant [16] and NP surface modification [17] are two other characteristics that have been discussed and may affect the tribological performance of nano-lubricants. According to various studies, when formulating nano-lubricants, an important factor is the concentration of NPs in the base oil [18]. Only a small amount of NPs is required to transform base oils to the required quality. The CoF and wear are at their lowest values at optimum concentration. If the NP concentration is altered in any of the directions, friction or wear will rise [19–37]. However, there is a lack of literature that examines how different mechanical characteristics of NPs, such as their material hardness, elastic modulus, and interfacial adhesion, affect the tribological behavior of nano-lubricant [38].

NPs added to the lubricant can be considered a closed three-body abrasive wear system where abrading particles (NPs) are contained between two surfaces and cannot escape easily. It is hypothesized that there is a critical role for the hardness and

concentration of NPs, which affect the anti-wear capabilities of nano-lubricants. The objective of this research is to investigate the effect of the hardness of the NP material and the NP concentration in the base oil on the anti-wear properties of nano-lubricant. The relative hardness of various materials is assessed using the Mohs hardness scale, which makes use of a group of ten reference minerals with numbers 1 through 10, with 1 being the softest and 10 being the hardest. Three materials, $CaCO_3$, TiO_2, and Al_2O_3, were selected for this investigation, having Mohs hardness values of 3, 6, and 9, respectively. These three materials cover a wide range of hardness and can be used as lubricant additives. The reason behind the selection of these nanoparticles in the present study is the longer wear life as an expression of durability, high plasticity, possible recrystallization, and film-forming tendency [39]. Furthermore, consideration has been given to the likelihood of achieving higher lubricity with these nanoparticles, which could lead to a significant reduction in friction, particularly at elevated temperatures. This potential reduction in friction opens the possibility of wider operational ranges, an important factor considered during the selection process [40]. As per Table 1, it is evident that a very small amount of nano-additives is sufficient to observe their anti-wear effect. To represent this spectrum, three concentrations, i.e., 0.1, 0.25, and 0.4 wt% of NPs in base oil, are selected for further investigation. The novelty of this work lies in its comprehensive exploration of the interplay between nanoparticle material hardness and concentration, specifically within the realm of nano-lubricants' anti-wear performance. By investigating the intricate relationship between these factors, the study unveils nuanced insights into how variations in material properties and concentration levels influence wear behavior, offering crucial guidance for optimizing nanoparticle-based nano-lubricants' anti-wear properties.

Methods

Jojoba oil

Jojoba oil being inert in nature exhibits low reactivity with either friction surfaces or nanoparticles. It is a non-polar oil with excellent chemical stability. In the present study, Jojoba (Simmondsia chinensis) oil was purchased from Kelkar Foods & Fragrance, Pune, India. The physicochemical characteristics of jojoba oil are summarized in Table 2.

Synthesis and characterization of NPs

Numerous synthesis approaches such as sol gel [45], wet chemical [46], and hydrothermal/solvothermal [47] methods are being practiced for the production of metal oxide nanoparticles [48]. The hydrothermal synthesis method was selected owing to various advantages [49]. Control over size and shape of synthesized particle, high purity of synthesized materials makes it a popular and versatile technique in nanotechnology [48, 50, 51]. Moreover, uniform particle distribution achieved with scalable production applying mild reaction conditions were the points considered while selecting the hydrothermal synthesis method in the production of nanoparticles in the present work. The nanometric powder samples of $CaCO_3$, TiO_2, and Al_2O_3 were synthesized by an atypical hydrothermal synthesis approach. AR grade nitrates of respective metal nitrates were procured from Sigma-Aldrich. Three separate batches with the same production protocol were carried out. Corresponding metal nitrate solutions were realized by dissolving

Table 1 Literature review

Sr. No	Base liquid lubricant	Nanoparticle material	Size (nm)	Nanoparticle concentrations (wt.%)	Optimum concentration (wt.%)	Reference
1	Mineral oil	Al_2O_3/SiO_2	70	0, 0.05, 0.1, 0.5, and 1.0	0.5	[19]
2	Pristine lubricating oil	Al_2O_3, TiO_2, Al_2O_3/TiO_2	75	0, 0.05, 0.1, 0.5, and 1.0	0.1	[20]
3	Lubricant oil	$ZnAl_2O_4$	95	0.05, 0.1, 0.5, and 1.0	0.1	[21]
4	SN 650 oils	Cu	10–15	0, 0.1, 0.15, 0.175, 0.5, and 1.0	0.15	[22]
5	Distilled water	Cu/SiO_2	20	0,0.5, 1.0, 1.5, and 2.0	1.0	[23]
6	Diesel engine oil (grade: 50 CC)	Serpentine	1.0 µm	0, 0.5, 1.0, 1.5, and 2.0	1.5	[24]
7	Fluoro silicone oil	LaF_3	10–30	0, 0.02, 0.04, 0.06, 0.08, and 0.1	0.08	[41]
8	EOT5# engine oil	SiO_2/MoS_2	30	0, 0.5, 1, 1.5, and 2.0	1.0	[25]
9	Multialkylated cyclopentanes (MACs)	Mo and W	20–50, 30–60	0.1, 0.5, and 1.0	0.5	[26]
10	Castor oil	TiO_2		0, 0.1, 0.2, and 0.3	0.2	[27]
11	Mineral oil	Al_2O_3	78	0, 0.05, 0.1, 0.5, and 1.0	0.1	[28]
12	Rapeseed oil	TiO_2	20	0 to 4.0	0.25	[29]
13	Paraffin oil	TiO_2	40	0.1 to 1.0	0.25	[30]
14	Engine oil	TiO_2	10–25	0.3, 0.4, and 0.5	0.4	[31]
15	PAO oil	Nanodiamond	4–5	0.01, 0.015	0.01	[32]
16	5W-30	Cu and Gr	10–20	0.03, 0.2, 0.4, 0.6	0.3	[33]
17	Engine oil	Al_2O_3 and TiO_2	8–12	0.05, 0.1, 0.25, 0.5	0.25	[34]
18	10 W-30	TiO_2	-	0.01, 0.25, 0.05, 0.075	0.075	[15]
19	Shorea Robusta oil	CuO	40	0.25, 0.5, 1.0	0.5	[35]
20	Madhuca indica oil	SiO_2	35	0.4, 0.8, 1.2	0.8	[36]
21	Engine oil	MoS_2	53	0.005, 0.01, 0.05, 0.1	0.01	[37]
22	PAO oil	Field's alloy nanoparticles	20	0.02, 0.04, 0.06, 0.08, 0.1	0.08	[42]
23	PAOs	MWCNTs	20–30	0.025, 0.05, 0.075, 0.10, and 0.15	0.075	[43]

a specific amount of metal nitrate in deionized water. Ethylenediamine was blended into metal nitrate solutions under the influence of vigorous stirring in the present hydrothermal synthesis approach. This inclusion was done since hydrothermal methods involve high temperatures and pressures, which can promote the formation of less stable species. Ethylenediamine works as a morphology control agent, preventing aggregation or precipitation and providing stability to metal complexes. It also eliminates the possibility of impurities or secondary phases [52, 53]. The resultant liquid was then blended with hydrazine (N_2H_4) to control the oxidation state. The solution was treated at 140 °C for 24 h in an autoclave with a 500-ml capacity. Consequently, the slurry was brought to

Table 2 Physicochemical properties of Jojoba oil [44]

Properties	ASTM standard	Jojoba oil
Density (kg/m3 @ 20 °C)	D1298	905
Kinematic viscosity (cSt)	D446-79	
at 40 °C		24.75
at 100 °C		6.43
Viscosity index	D2270-79	233
Lower heating of value (kJ/kg)	D 240	38,100
Flash point (°C)	D92-85	275
Fire point (°C)	D287-82	322
Cloud point (°C)	D2500-16a	24
Pour point (°C)	D97-85	8

room temperature by placing it in ambient conditions. To get rid of possible impurities, three cycles of centrifugation-washing with distilled water and ethanol were conducted. The resultant powder was heat treated at 300 °C for 6 h to produce nano-regime crystallites. The phase and stoichiometrically confirmed samples were subjected to tribological testing.

The confirmation of the chemical constituent correctness, crystallinity, and crystalline grain size of the prepared nano-powders was achieved. The characterization specifications of X-ray diffraction were a 2θ range 20–60°, incremental parameter of 0.005, and a counting interval of 100 s on a Bruker X-ray diffractometer (Model D2 PHASER) with CuKα. The phase identification was performed and compared to the standard JCPDS diffraction patterns 00–005-0586, 21–1272, and 96–120–0006 and 96–101–0462 for $CaCO_3$, TiO_2, and Al_2O_3, respectively [54–56]. The vital information about crystallinity and chemical constituent correctness was evaluated by comparing the areas under the 100% zeniths, getting rid of the background error. The confirmation of the stoichiometric correctness and complexation of the synthesized specimens was conducted using the energy dispersive X-ray analysis (EDX) technique. Scanning electron microscope (SEM) images of the specimens were recorded on TESCAN (Model MIRA3 LMH). The samples were coated with gold for better conductivity on the specimen surface.

The zenith peak positions and intensity of a sample in the XRD pattern when compared with diffraction database reference provide the confirmation about phase and crystallinity and help in quantifying the composition of nanoparticles. XRD zenith peaks of $CaCO_3$, TiO_2, and Al_2O_3 nanoparticles are shown in Figs. 1a, 2a, and 3a. The presence of strong-intensity zenith peaks was an indication of the fact that formed nanoparticles possessed a crystalline structure. The zenith peaks observed in all three diffraction patterns were as mentioned in the respective JCPDS cards. The full width at half maximum of all zenith peaks was used to estimate average crystallite sizes. The calculated values indicated that they were composed of small-size crystallites. The average particle size for respectively for $CaCO_3$, TiO_2, and Al_2O_3 was found to be 32.7, 35.1, and 33.6 nm, and detailed specifications of NPs are provided in Table 3. The corresponding specific surface area values calculated were in the range of 48 to 53 m^2/g. The perceptive observation of specimen surface morphology (SEM) is presented in Figs. 1b, 2b, and 3b. The SEM images present tufted well-faceted solid bodies with

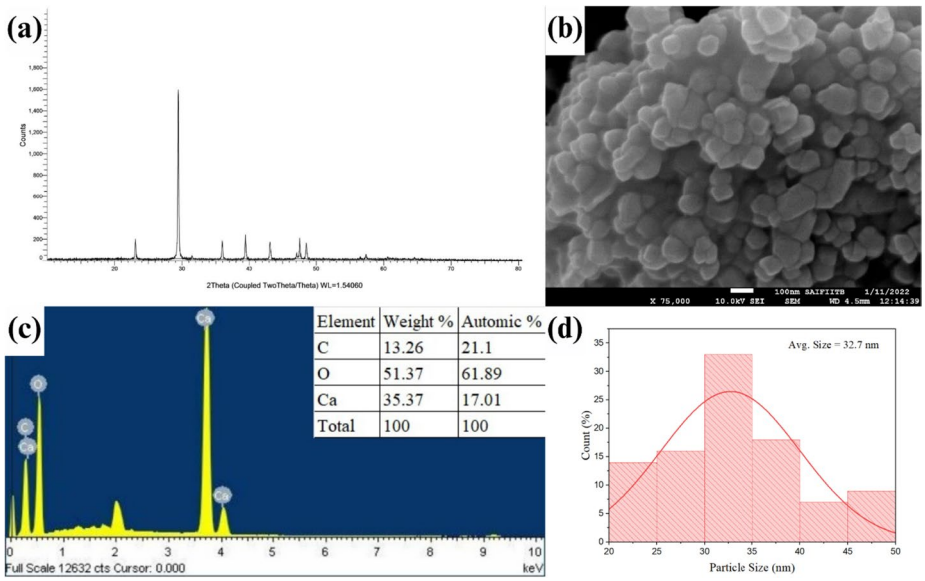

Fig. 1 **a** XRD, **b** SEM, **c** energy dispersive, and **d** particle size distribution of $CaCO_3$ nano-additive

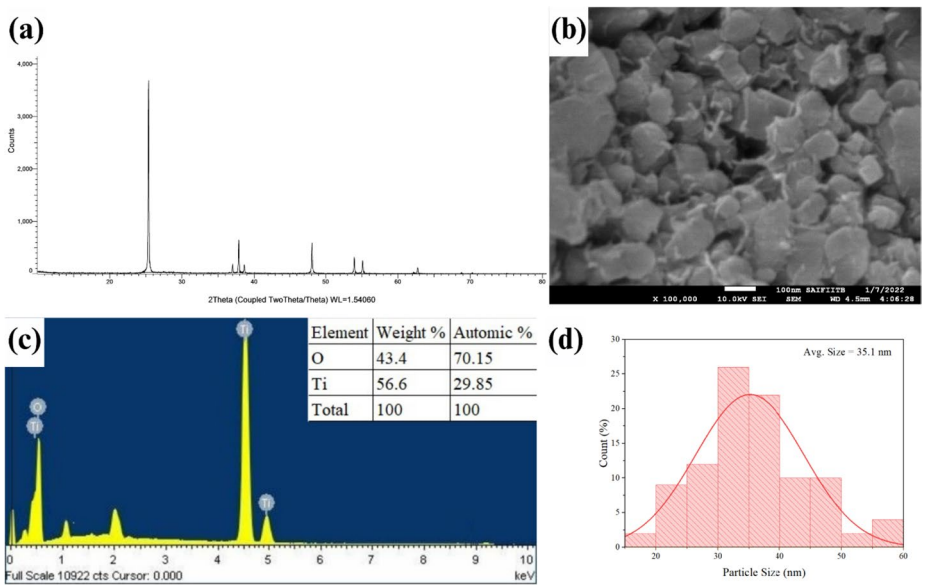

Fig. 2 **a** XRD, **b** SEM, **c** energy dispersive, and **d** particle size distribution of TiO_2 nano-additive

cloudy, homogeneous microstructure which may be associated with the fact that heat treatment as a part of the production protocol resulted in grain growth. The recorded SEM images revealed the presence of agglomerated nanoparticles that exhibited a nearly spherical shape. The stoichiometric compositional correctness of the prepared specimens carried out by EDX is presented in Figs. 1c, 2c, and 3c. This was conclusive evidence about the precise match between the desired and final product stoichiometry having an accurate percentage of each element in the prepared specimens, ensuring their purity.

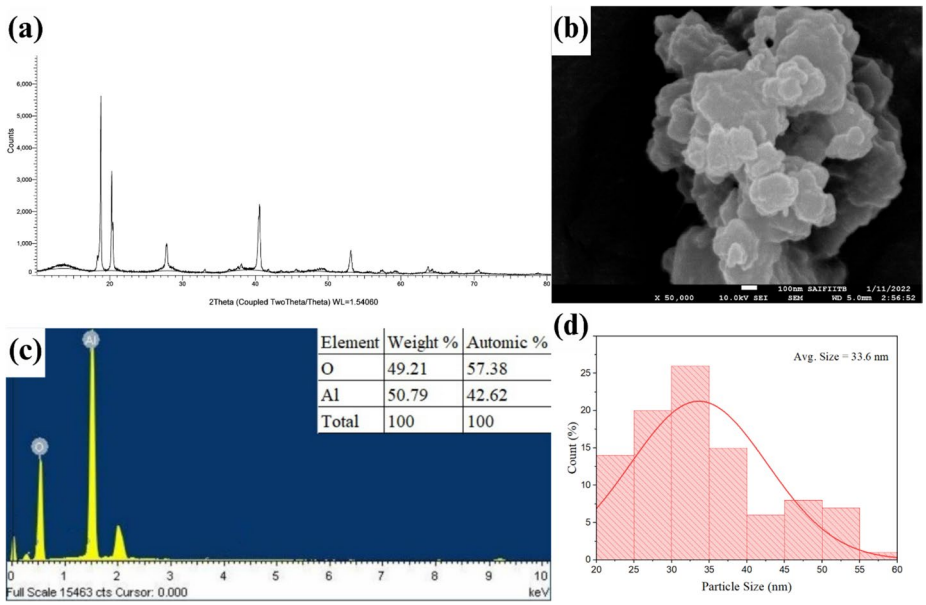

Fig. 3 **a** XRD, **b** SEM, **c** energy dispersive, and **d** particle size distribution of Al_2O_3 nano-additive

Table 3 Specifications of $CaCO_3$, TiO_2, and Al_2O_3 NPs

Property	$CaCO_3$	TiO_2	Al_2O_3
Morphology	Rhombohedral	Rhombohedral	Rhombohedral
% Purity	100%	100%	100%
Average particle size (nm)	32.7	35.1	33.6
Molar mass (g/mole)	100.09	79.87	101.96
Specific surface area (m^2/g)	52	48	53
Bulk density (g/cm^3)	2.71	4.23	3.95
Bulk hardness, Mohs	3	6	9

Sample preparation

Jojoba oil, being a slightly acid medium with good flotation properties, is a useful base oil in a uniformly dispersed nanofluid [57, 58]. The laboratory-synthesized nanoparticles, along with jojoba oil obtained without further purification, were used to prepare the nanofluid by the synthesis-dispersion approach. Reportedly, the enhancement of nanofluid stability has been achieved through various methods, including dispersant mixing, mechanical agitation via rotation, and/or sonication [59]. From a toxicity and environmental hazards point of view, the use of surfactants was avoided. In this study, both mechanical agitation and sonication were employed to ensure the efficient dispersion of nanoparticles within the base oil [60]. The nano-lubricant samples were realized by a synthesis-dispersion method with weight fractions (wt%) of 0.1%, 0.25%, and 0.4% of $CaCO_3$, TiO_2, and $Al2O_3$ NPs dispersed in jojoba oil. The solution of nanoparticles dispersed in base oil was subjected to continuous stirring (Remi 1 MLH 1Ltr Magnetic Stirrer) for 2 h with ~ 1500 rpm to get stable and homogenous nano-lubricant samples. After conducting mechanical agitation via stirring, the nanofluids were subjected to sonication (Ultrasonic Processor UP-100 Chrom Tech, Inc.) at a

frequency of 57 kHz for a duration of 1 h at ambient temperature. All the nanofluid specimens displayed good dispersion stability [61]. Figure 4 represents a schematic illustration of the synthesis of nanoparticles and preparation of nano-lubricants discussed in this section.

Tribological tests

The tribological performance from lone base oil to increased wt% samples of NPs was experimentally examined and further analyzed using the ASTM protocol D4172, laying the groundwork for all the experimental variations. A DUCOM TR-30L four-ball tribo-tester was utilized to record the tribological performance. Bearing steel class balls with the specifications of a high-carbon chromium alloy, AISI 52100, a diameter of 12.7 mm, and a hardness of 64 HRC were used. Test balls were cleared with acetone to ensure the ball surface was free from any contaminants, surface oxidation, corrosion, or organic remnants. The tribo-tester was loaded with these cleaned balls, and 10 ml of sample fluid was filled in the oil cup. The test parameters, such as rotating speed and load, were maintained constant, and tests were carried out as a function of wt% concentrations of NPs. The test specifications were maintained as follows: time interval = 3600 s; temperature = 75 °C; force = 40 kgf; spindle speed = 1200 rpm. In this test rig, an additional fourth ball was held in a spinning spindle of three balls. The three balls were held inanimately in a ball pot. Figure 5 shows the ball pot assembly of the four-ball tribometer test rig used in the present study, along with a schematic representation of the four-ball tester. A precise optical comparator (VMM; Sipcon-SVI-IMG-3D) was used to note the wear caused on the three stationary balls. This was instrumental in measuring the wear scar diameter (WSD). The visualization and measurements of the wear scar were carried out with the help of professional software. The presence of trace elements on wear scar surfaces and the topography of the worn surfaces were analyzed by energy dispersive spectrometry (EDS-JEOL—JSM-6380) and atomic force microscopy (AFM-Perk Systems; XE-7) respectively. Surface morphological parameters such as shape, roughness, and topographic variations at the nano-scale level were evaluated using AFM.

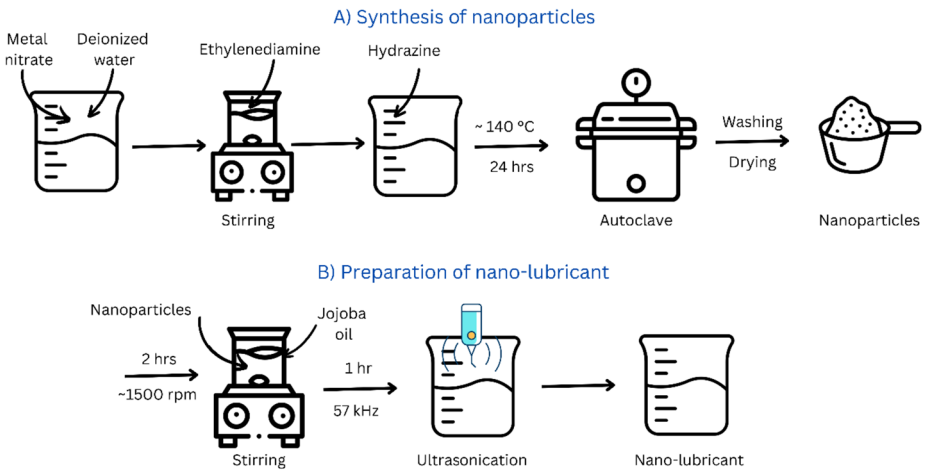

Fig. 4 Schematic illustration of **a** synthesis of nanoparticles and **b** preparation of nano-lubricant

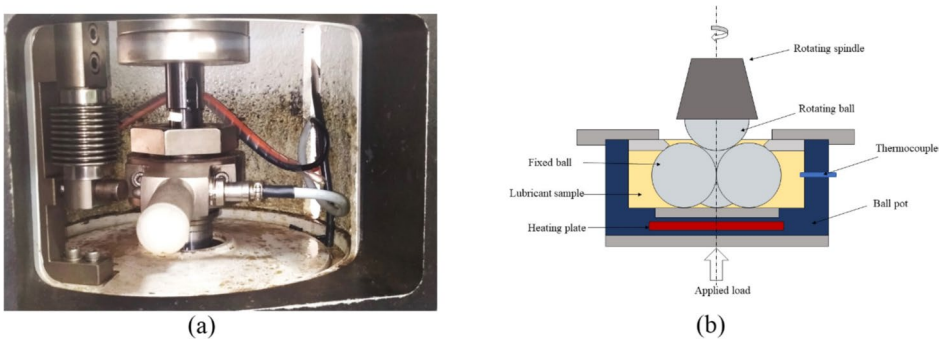

Fig. 5 **a** Ball pot assembly of four-ball tribo-tester and **b** conceptual illustration of four-ball tribo-tester

Table 4 Factors and levels for experiments

Factors	Parameters (unit)	Levels		
		−1	**0**	**1**
H	Hardness (Mohs)	3	6	9
C	Concentration (wt%)	0.1	0.25	0.4

Design of Experiments (DoE)

The term "design of experiments" (DoE) refers to a technique for planning experiments and reviewing the results. The method enables the use of a minimal number of trials, in which multiple experimental parameters are simultaneously and methodically modified to gather sufficient data. A computational representation of the process under study can be developed based on the collected data. The factors that are crucial for understanding process variation can be found with the use of DoE. Another advantage of DoE is to understand how the influencing factors interact with one another. RSM is utilized in the current work to examine how input factors affect response parameters. RSM is a group of mathematical and statistical methods applied for modeling and analysis when an outcome variable is affected by numerous explanatory variables. In RSM, the independent variables, or predictor variables, are mainly known as the factors, while the dependent variables are known as the responses [62]. Central composite design (CCD) is a popular technique for designing response surfaces. With additional center points and the axial points, also known as star points, the CCD is a two-level full factorial design. Tables 4 and 5 offer a central composite design (CCD) with two factors and six replications at the center with an alpha value of 1. The four-ball tester has been used to conduct tribological experiments in accordance with the DOE design matrix shown in Table 5, and the appropriate findings have been recorded. The WSD provided here is the arithmetic mean of the measured values from each test, which was carried out three times under identical experimental conditions. The analysis is performed using Minitab® 16 software, and the CCD technique is utilized to arrange the experiments.

Table 5 Central composite design (coded factors)

Std. order	Run order	Blocks	Factors	
			H	C
1	6	1	−1	−1
2	2	1	1	−1
3	5	1	−1	1
4	1	1	1	1
5	7	1	0	0
6	3	1	0	0
7	4	1	0	0
8	9	2	−1	0
9	13	2	1	0
10	10	2	0	−1
11	12	2	0	1
12	11	2	0	0
13	14	2	0	0
14	8	2	0	0

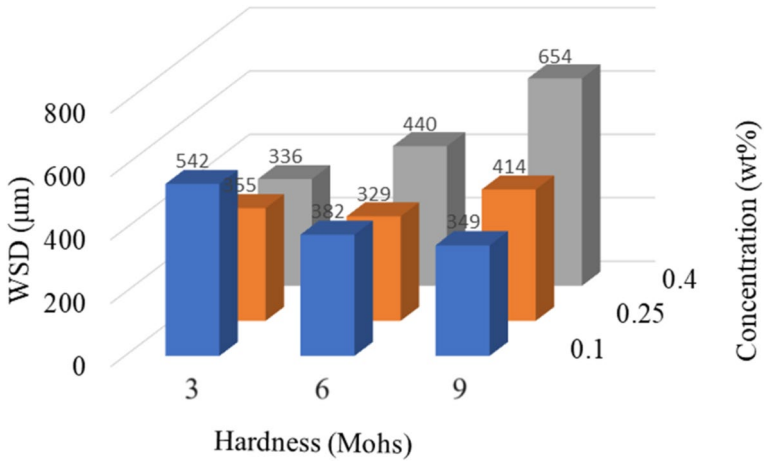

Fig. 6 Experimental results

Results and discussion

According to the DoE design matrix provided in Table 5, tribological experiments have been carried out using the four-ball tester, and the appropriate findings have been recorded. The results are shown in Fig. 6. The largest value of WSD is observed for harder material (Al_2O_3) with a high NP concentration (0.4 wt%) whereas the smallest value of WSD is observed for moderately harder material (TiO_2) with a moderate level of NP concentration (0.25% wt%). The WSD on three balls for a specific trial are shown in Fig. 7.

Table 6 shows the ANOVA analysis of WSD for three nano-lubricants with varying hardness of NP material and concentration of NPs in the base oil. It provides an overview of each factor's impact as well as how they interact when fitted into a second-order quadratic model. The model is created using an adequate model reduction with a 95% confidence

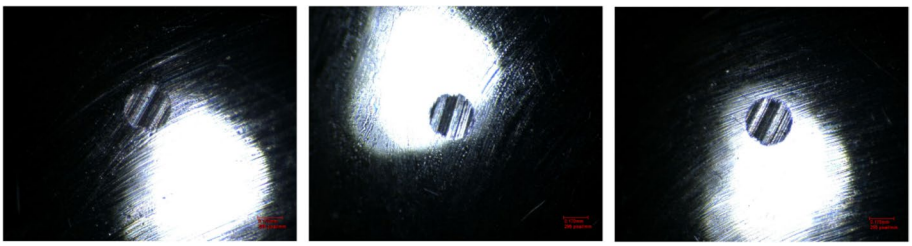

Fig. 7 WSD for a specific trial (Std order 6 — base oil containing 0.25 wt% of TiO_2)

Table 6 Analysis of variance (ANOVA) for WSD

Source	DF	Adj SS	Adj MS	*F*-value	*P*-value	VIF
Model	6	123,898	20,649.7	6251.69	0.000	
Blocks	1	1	1.3	0.39	0.551	
Linear	2	9493	4746.7	1437.05	0.000	
Hardness	1	5643	5642.7	1708.31	0.000	1.00
Concentration	1	3851	3850.7	1165.79	0.000	1.00
Square	2	43,604	21,802.2	6600.61	0.000	
Hardness*hardness	1	8594	8593.5	2601.68	0.000	1.26
Concentration*concentration	1	19,766	19,766.4	5984.27	0.000	1.26
2-way interaction	1	65,280	65,280.3	19,763.56	0.000	
Hardness*concentration	1	65,280	65,280.3	19,763.56	0.000	1.00
Error	7	23	3.3			
Lack-of-fit	3	16	5.5	3.29	0.140	
Pure error	4	7	1.7			
Total	13	123,921				

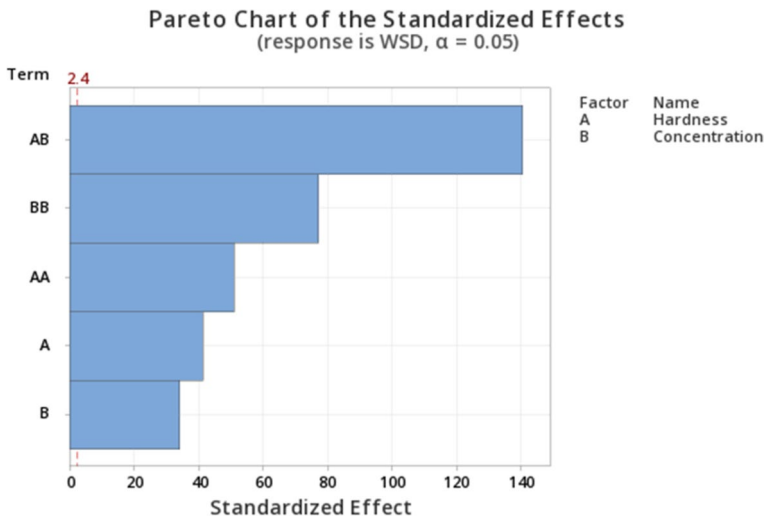

Fig. 8 Pareto chart for standardized effect

level. The Pareto chart in Fig. 8 shows the values of the standardized effects in descending order of value. The chart additionally includes a reference line with a value of 2.4 indicating which factors are statistically significant; all factors greater than this value of 2.4 are statistically significant. As per the Pareto chart, the interaction between hardness and concentration is the most significant. The individual effects of hardness and concentration are far less important in controlling the WSD as compared to the interaction between these two factors.

Using the variance inflation factor (VIF), the predictor variables' multicollinearity is examined. The value for the VIF is shown in Table 6. All predictors' VIF values are reported to be around 1, indicating that there is no multicollinearity among the predictors. The model depicted in Table 6 is further tested for statistical accuracy to ensure its predictive power. The estimated coefficient of determination (R^2) for the model is 0.9998, which suggests that the model adequately captures the real relationships between the various experimental factors (Table 7). The normal probability plot of WSD is displayed in Fig. 9. The normal probability plot, which compares predicted and actual values for the design matrix, is the ultimate result of assessing the normality of the experimental results. It is clear from Fig. 9 that the residual values are quite low and closely confirm the mean line shown on the normal probability plot. Regression analysis is used to model and analyze several variables that include a response variable and two predictor variables. The hardness of the NP material (H) and the concentration of NPs (C) are predictor variables, while the WSD is a response variable. The predictive equation for WSD that was developed using regression analysis is given by Eq. (2).

$$WSD = 1112.18 - 135.59H - 3426.3C + 6.237H^2 + 3783.7C^2 + 283.89HC \quad (2)$$

The model results for WSD are validated with experimental results for the optimum value of NP concentration for all three NP materials. WSD for nano-lubricants is predicted using the predictive equation determined by ANOVA for WSD as presented in Eq. (2). Utilizing the experimental data, the results of the proposed mathematical association have been verified.

This polynomial equation can predict and optimize the WSD response value. Figure 10 depicts response surface optimization graphs obtained from response surface analysis and prediction. These graphs indicate the optimum value of concentration for a specific NPs i.e. harness value.

Table 8 compares the outcomes of the experiment with those that were predicted; the experimental values are very close to those predicted by the quadratic regression equation. The findings of the validation studies showed that the measured and predicted WSD values agreed well. Figure 11 shows the scatter plot between the actual (outcomes of the experiment) and predicted values of WSD, as points on the plot fall on a straight line, it indicates that the model is making accurate predictions.

Table 7 Model summary of the quadratic model for WSD

S	*R*-squared	Adjusted *R*-squared	Predicted *R*-squared
1.81743	99.98%	98.97%	98.87%

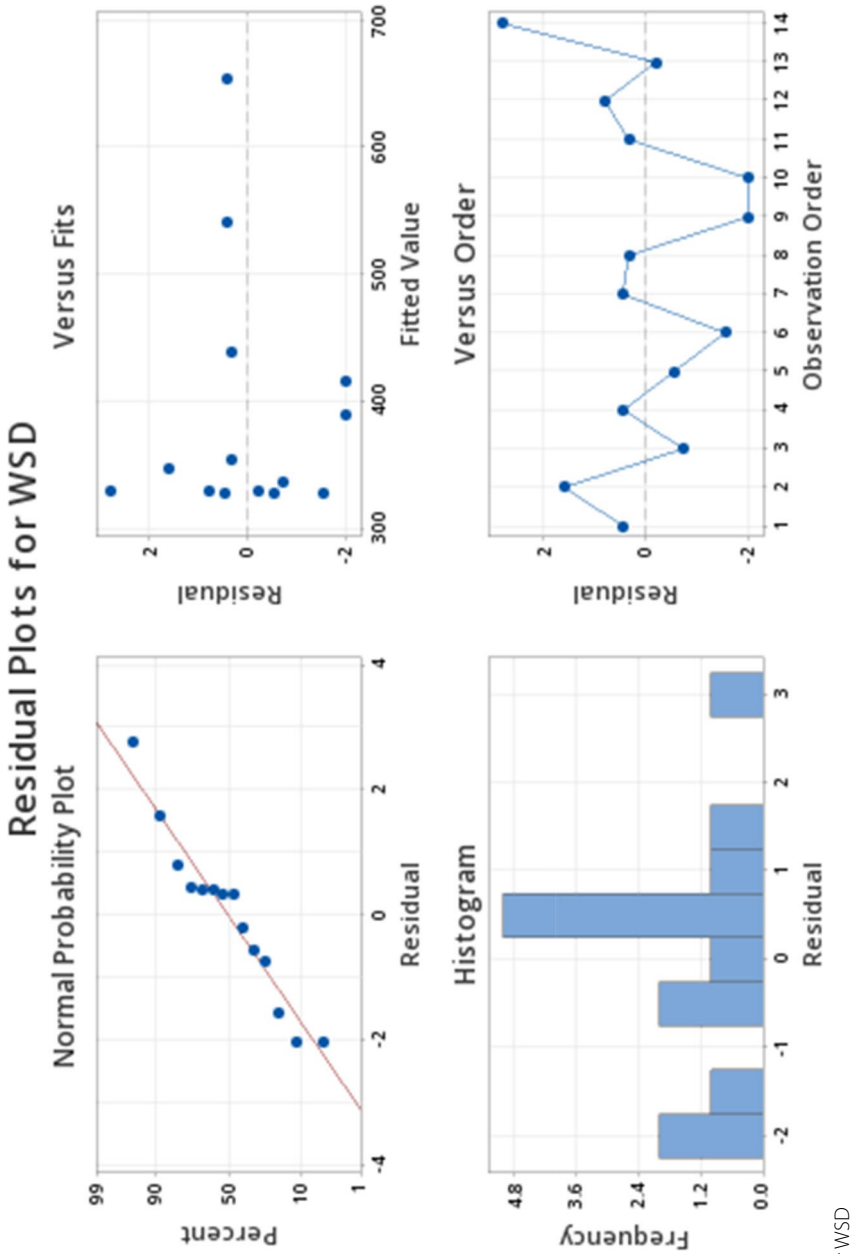

Fig. 9 Residual plots for WSD

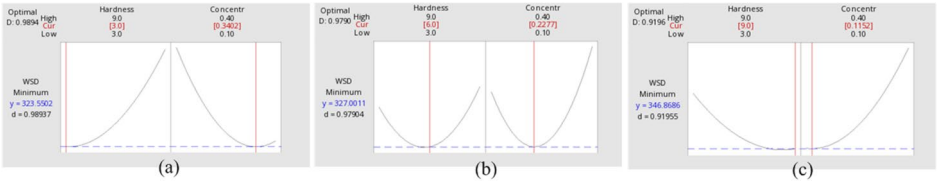

Fig. 10 Optimization graph of the WSD for **a** $CaCO_3$, **b** TiO_2, and **c** Al_2O_3 NPs

Table 8 Experimental validation results

NP material	Hardness (Mohs)	NP concentration (wt%)	WSD (μm)		
			Predicted	Experimental	% error
$CaCO_3$	3	0.3402	323	328	1.54
TiO_2	6	0.2277	327	335	2.44
Al_2O_3	9	0.1152	346	352	1.73

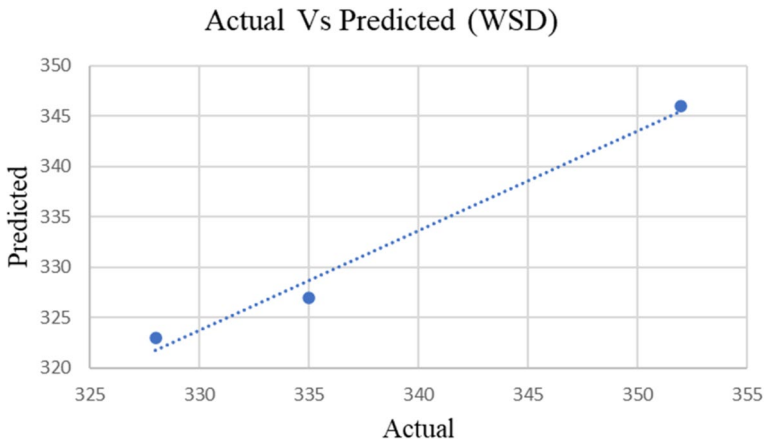

Fig. 11 The scatter plot between the actual and predicted values of WSD

As discussed in an earlier section, wear initially decreases as NPs concentration is increased up to a certain point in a tribological system using nano-lubricant, but as concentrations rise further, wear begins to increase [19–32, 41]. The main effect plot (Fig. 12) between NPs concentration and WSD shows similar findings for the chosen concentration range. A similar type of trend is observed for nanoparticle material hardness. However, as per the ANOVA analysis, the interaction between hardness and concentration is more vital than their individual contributions, so to understand this interaction, further analysis is carried out by plotting the interaction plot between hardness and concentration, showing the combined effect for WSD (Fig. 13).

For relatively softer material ($CaCO_3$), a high concentration (0.4 wt%) of NPs is required to achieve a similar wear reduction effect that harder materials (Al_2O_3) achieve at a much lower concentration (0.1 wt%). In contrast, harder material (Al_2O_3) with a high concentration (0.4 wt%) will increase wear more than normal. The contour plot and surface plot (Fig. 14) of WSD vs. concentration and hardness provide a clearer picture of the response.

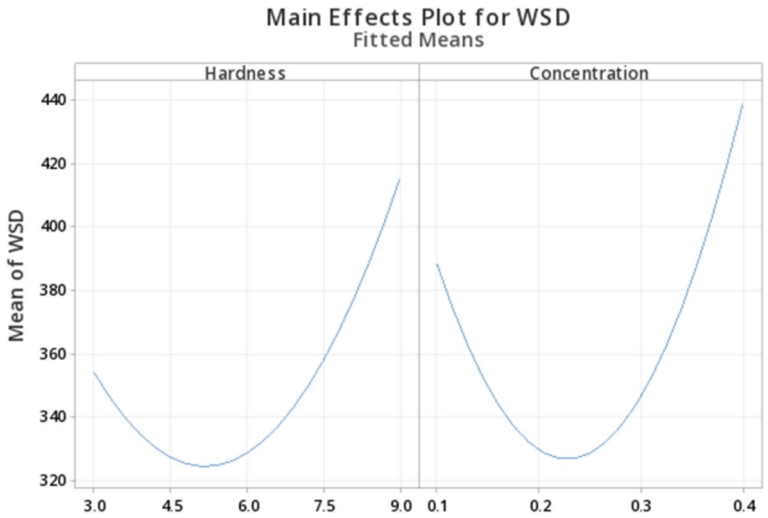

Fig. 12 Main effect plot for WSD

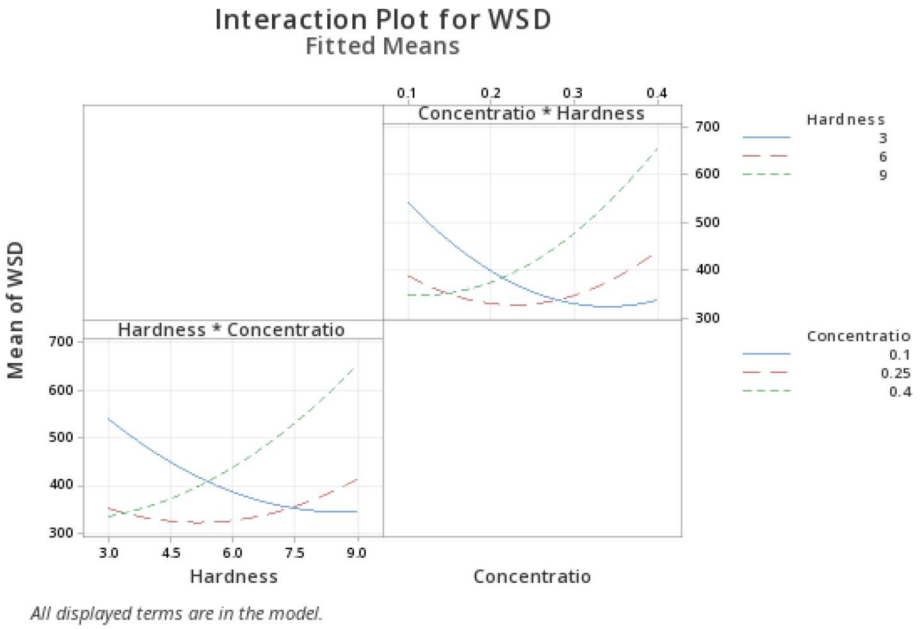

Fig. 13 Interaction plot for WSD

To determine whether the given combination of hardness and concentration is promoting or preventing wear, a trial was conducted in accordance with ASTM D4172 using pure base oil without including NPs; the WSD for this trial was 561 µm. Figure 15 indicates two regions separated by the critical value of WSD obtained for pure base oil. Any value of hardness and concentration within the blank region will result in a lower WSD than the critical value and demonstrate anti-wear behavior, whereas values in the gray region will result in a greater WSD than the critical value, demonstrating third-body wear behavior.

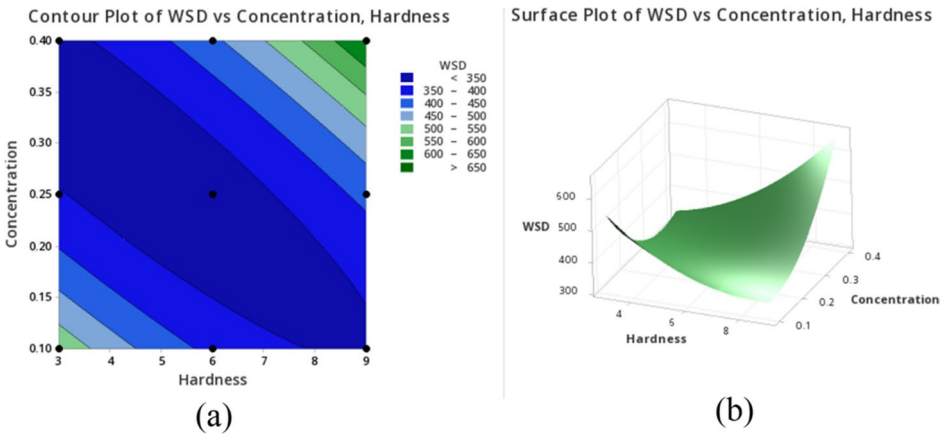

Fig. 14 **a** Contour plot and **b** surface plot for WSD vs concentration and hardness

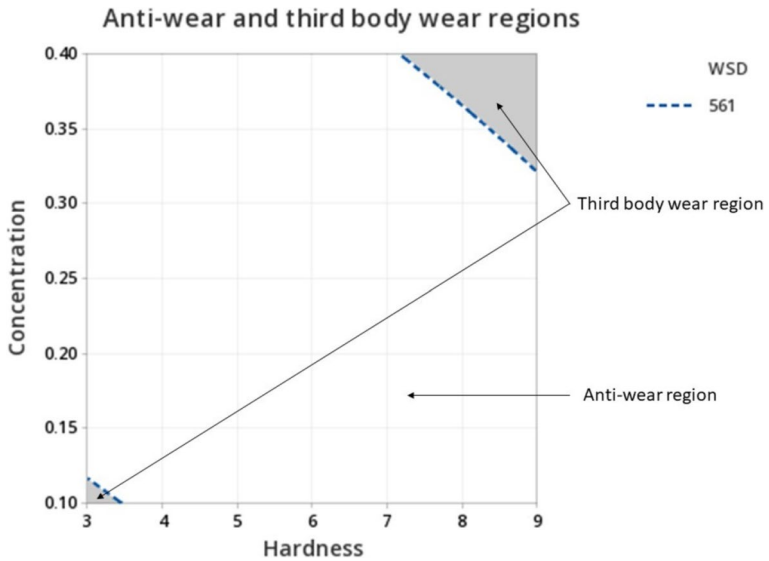

Fig. 15 Anti-wear and third-body wear regions

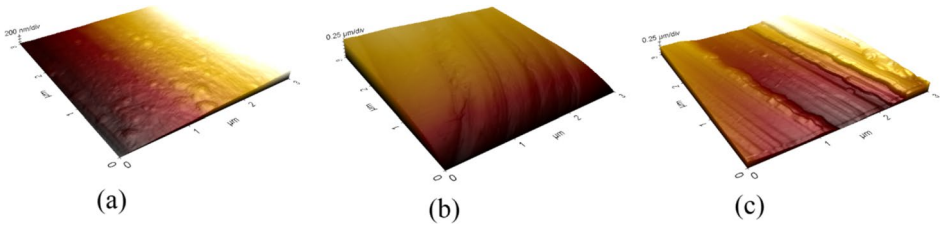

Fig. 16 AFM of worn surface on ball with 0.4 wt% of **a** $CaCO_3$, **b** TiO_2, and **c** Al_2O_3NPs

To further understand the change in wear mechanism with changes in nanoparticle concentration and hardness, AFM and EDS analysis of the scuffed ball surfaces are used. Figure 16 illustrates the topography of scuffed ball surfaces for each nano-lubricant sample at its highest concentration of NPs. With nano-lubricant containing

Al_2O_3 NPs, there are dense parallel grooves on the worn surface in the sliding direction (Fig. 16c). These grooves on the surface may have been generated by the inclusion of NPs in the oil, which have caused some abrasion due to their hard nature, whereas there are thin parallel grooves on the worn surface for nano-lubricant containing TiO_2 NPs due to its relatively soft nature (Fig. 16b). Interestingly, there are no signs of any abrasive wear for nano-lubricants containing $CaCO_3$ NPs (Fig. 16a).

For the oil blended with the highest concentration (0.4 wt%) of Al_2O_3 NPs, surface damage is comparatively severe. The reason for the wear in this instance could be the scratching damage caused by the abrasive action of NPs trapped between oppositely interacting surfaces. Also, the WSD value for this concentration is 654 µm which is even higher than the WSD for pure base oil (561 µm) suggesting that this higher level of concentration and hardness leads to third-body wear instead of preventing it. To verify whether the dense grooves on the surface (Fig. 16c) are the result of abrasive wear due to Al_2O_3 NPs, an X-ray microanalysis of the scuffed surface was performed. After being tested for all three concentrations of Al_2O_3 NPs, the worn-out balls were washed with acetone to remove oil and any loose NPs. Then, they were analyzed using EDS to see if any NPs had been indented over the worn-out surface of the ball. A peak of the element Al may be seen in the EDS spectra of the worn-out surfaces for base oil containing 0.4 wt% of Al_2O_3, indicating the existence of Al_2O_3 (Fig. 17b), whereas there are no traces of Al for lower concentrations of Al_2O_3 NPs in base oil (Fig. 17a). EDS analysis of pristine samples was also conducted. This would allow for a meaningful comparison of the chemical composition before and after sliding. The samples before sliding had only chromium, carbon, iron, and oxygen peaks confirming the balls used were free from trace elements and impurities.

It could be inferred from the above analysis that, at higher concentrations, NPs of harder material (Al_2O_3 ~ 9 Mohs) get indented over the softer ball surface (AISI 52100 steel ball of 64 HRC ~ 6 Mohs) and cut the opposite surface, which enhances the wear on both sliding surfaces. However, this indentation of NPs over the ball surface is not observed at lower concentrations of Al_2O_3 NPs or at higher concentrations of $CaCO_3$ and TiO_2, and it could be attributed to the lower and similar hardness of these nanoparticle materials compared to test balls. If there are enough abrasive particles and their hardness is higher than the sliding surfaces, they will indent over the softer

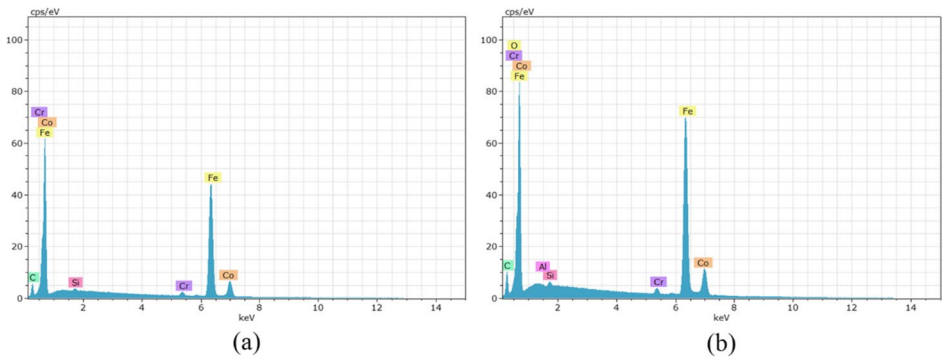

Fig. 17 EDX of worn surface on ball for Al_2O_3 nanoparticle with **a** 0.25 wt% and **b** 0.4 wt%

sliding surface and cut the opposing surface. On the other hand, the harder sliding surfaces crush the softer abrasive particles.

Several lubrication mechanisms have been put forth in recent years to explain how the lubrication effect has improved because of the addition of various NPs in a lubricant. These mechanisms include the development of protective films [63, 64], superior adsorption [65], the ball-bearing effect, the mending effect, and the polishing effect. The mending and polishing effect improves the quality of the surface [12, 66, 67]. Nanoparticle deposition occurs on rubbing surfaces as well as worn surfaces and fills grooves during mending or self-repairing mechanisms (Fig. 18a). This effect is specifically observed for NPs of softer materials. Figure 16a indicates a similar lubrication mechanism for the nano-lubricant with the highest concentration of $CaCO_3$ NPs; similar results are reported for MoS_2 NPs dispersed in PAO oil; the smoother wear surface was attributed to the "filling" of the little pits by the NPs [68]. The "polishing effect," also known as the smoothing effect, is thought to be observed when the lubricating surface's roughness is decreased through abrasion assisted by NPs (Fig. 18b). The thin parallel grooves on the worn surface for nano-lubricant containing TiO_2 NPs (Fig. 16b) resemble the polishing effect, similar effects have been reported for TiO_2 nano-additives in water-based lubricants and mineral oils [69, 70], whereas scratching due to "abrasive wear" is observed in case of Al_2O_3 NPs at higher concentrations (Fig. 18c).

Surface chemistry plays a crucial role in the formation of tribo-films at the interface and, consequently, influences wear in tribological systems [71]. The chemical interactions occurring at the sliding interface would differ as well, resulting in the formation of chemically different tribo-films and wear behaviors [72]. Besides nanoparticle hardness, the surface chemistry of each material was also taken into consideration as it is subject to change as these materials are distinct in their chemical behavior. As the involved nanoparticles were oxides in all the three cases, the formation of the oxide tribo-films was attributed as protective layers against further wear. The chemical affinity between surfaces affects adhesion and friction [73]. Strong adhesive forces can lead to material transfer between surfaces and the formation of tribo-films. The chemical compatibility of materials also influences the frictional forces at the interface. These factors can affect the spreading and adhesion of lubricants and additives, influencing the formation and stability of tribo-films.

The scenario of boundary lubrication conditions may evolve as an adsorption film and/or a tribo-chemical reaction film formed between the two contact surfaces. The formation of the adsorption film results from the polar groups which can be strongly adsorbed onto the metal surface at the molecular layer. Since the jojoba oil does not contain polar groups, the contained unsaturated hydrocarbons have a certain adsorb ability onto the metal surface, it can be considered that in this experiment it is mainly Ca_2+, Ti_4+, and

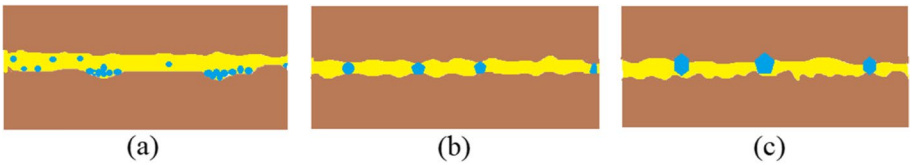

Fig. 18 **a** Mending effect. **b** Polishing effect. **c** Abrasive wear

Al_3+ can be adsorbed onto metal surface. All Ca_2+, Ti_4+, and Al_3+ have up to 6 polar groups in a coordination complex derivative [74]. The direct contact of the two friction surfaces is reduced effectively and the friction coefficient is lowered when the maximum number of molecules are adsorbed, and the free energy of the metal surface is minimized [75]. The structural and chemical composition of the tribo-film could be further assessed by a high-resolution electron microscope approach and electron energy loss spectroscopy (EELS) or by employing an electrochemical workstation [76].

Selecting nanoparticles for lubricating oil additives requires careful consideration of their distinct properties, compatibility with the lubricant, and their intended application to ensure optimal machinery or component performance and longevity. Considering the study's findings, Al_2O_3 nanoparticles emerge as particularly effective additives for enhancing anti-friction and anti-wear properties in lubricating oils, attributed to their exceptional hardness and wear-resistant nature. Even a minimal amount of doping with these nanoparticles proves sufficient to create protective coatings, reduce friction between moving parts, and significantly bolster the durability of lubricated surfaces. However, it is noteworthy that an increase in nanoparticle concentration correlates with heightened wear, posing challenges in situations where controlling this concentration becomes difficult. Moreover, when dealing with soft surfaces, Al2O3 NPs may not be the most suitable choice, as they tend to penetrate such surfaces and potentially cause damage. In contrast, TiO_2 and $CaCO_3$ nanoparticles, being softer materials, offer a better alternative in scenarios where one or both contacting surfaces are softer, mitigating the risk of penetration and damage to the opposing surface.

The cost-versus-performance analysis of the produced nano-lubricant serves as a critical determinant in justifying the commercialization of the product. A comprehensive examination comparing the cost-effectiveness and performance enhancement achieved by incorporating nanoparticles like calcium carbonate ($CaCO_3$), titanium dioxide (TiO_2), and aluminum oxide (Al_2O_3) into the lubricant can establish a compelling case for commercial viability. Calcium carbonate stands out as the most cost-effective among other NPs due to its abundant natural availability and lower production expenses. Widely used across industries like paper, plastics, paints, and coatings, it offers cost efficiency, acts as a filler, and exhibits white pigment properties. With its cost-efficiency and moderate performance, it might offer an economically favorable option, while TiO_2 and Al_2O_3, despite their potential superior performance, could incur higher production costs due to expensive extraction and refinement processes. A detailed study evaluating the balance between the cost of nanoparticle incorporation and the resultant enhancement in lubrication performance will be pivotal in determining the commercial feasibility of the nano-lubricant.

Conclusions

The comprehensive exploration of nanoparticle material hardness and concentration on anti-wear performance in nano-lubricants reveals pivotal insights. Evaluating $CaCO_3$, TiO_2, and Al_2O_3 nanoparticles elucidates their relationship with wear behavior, emphasizing the interplay between material properties and wear reduction efficacy. While softer $CaCO_3$ requires higher concentrations for comparable wear reduction achieved by harder Al_2O_3 at lower concentrations, higher concentrations

of harder materials, like Al_2O_3, unexpectedly promote wear. Surface analysis techniques showcase that increased concentrations of harder nanoparticles accelerate wear, contrasting the surface mending and polishing effects of softer nanoparticles that improve surface quality and reduce wear.

Surface chemistry profoundly influences tribo-film formation, serving as a crucial factor in tribological systems. Beyond nanoparticle hardness, consideration of distinct surface chemistry, especially in oxide nanoparticles, reveals their role in forming protective tribo-films. Chemical interactions between surfaces affect adhesion, friction, and material transfer, influencing tribo-film stability. Polar groups in boundary lubrication facilitate adsorption onto metal surfaces, decreasing direct contact and friction coefficients. Further analysis using high-resolution electron microscopy and spectroscopy methods can deepen our understanding of tribo-film composition.

In summary, while Al_2O_3 nanoparticles excel in enhancing lubrication, their higher concentrations pose increased wear risks on softer surfaces. For softer surfaces, TiO_2 and $CaCO_3$ serve as safer alternatives. $CaCO_3$ stands out as cost-effective due to its abundance, whereas TiO_2 and Al_2O_3 may involve higher production expenses. This study emphasizes the need for a balanced consideration of material properties, concentration, and surface chemistry to optimize nanoparticle-based anti-wear performance for practical applications in lubrication systems.

Abbreviations

AISI	American Iron and Steel Institute
ANOVA	Analysis of variance
AR	Analytical research
ASTM	American Society for Testing and Materials
AW	Anti-wear
CCD	Central composite design
CoF	Coefficient of friction
DOE	Design of experiments
EDX/EDS	Energy dispersive X-ray analysis
HRC	Hardness on Rockwell scale C
JCPDS	Joint Committee on Powder Diffraction Standards
NPs	Nanoparticles
RSM	Response surface methodology
SEM	Scanning electron microscope
WSD	Wear scar diameter
wt%	Weight fractions
XRD	X-ray diffraction

Acknowledgements
Not applicable

Authors' contributions
TK conceptualized the study, conducted the experimentation, wrote the original draft, analyzed the data, and reviewed the article. BT contributed to the synthesis and characterization of nanoparticles. AA has contributed to developing the methodology, writing, and reviewing the article. All authors have read and approved the manuscript.

Funding
The authors declare that no funds, grants, or other support were received during the preparation of this manuscript.

Availability of data and materials
The datasets used and/or analyzed during the current study are available from the corresponding author on reasonable request.

Declarations

Competing interests
The authors declare that they have no competing interests.

Received: 21 November 2023 Accepted: 17 January 2024
Published online: 02 February 2024

References

1. Li Y, Schreiber P, Schneider J, Greiner C (2023) Tribological mechanisms of slurry abrasive wear. Friction 11(6):1079–1093. https://doi.org/10.1007/s40544-022-0654-1
2. Williams JA, Hyncica AM (1992) Abrasive wear in lubricated contacts. J Phys D Appl Phys 25(1A):A81–A90. https://doi.org/10.1088/0022-3727/25/1A/015
3. Xuan JL, Hong IT, Fitch EC (1989) Hardness effect on three-body abrasive wear under fluid film lubrication. J Tribol 111(1):35–40. https://doi.org/10.1115/1.3261876
4. Archard JF (1953) Contact and rubbing of flat surfaces. J Appl Phys 24:981–988. https://doi.org/10.1063/1.1721448
5. Dwyer-Joyce, R. S. (1993). The effects of lubricant contamination on rolling bearing performance. Retrieved from http://spiral.imperial.ac.uk/handle/10044/1/8943
6. Bhaumik S, Datta S, Pathak SD (2017) Analyses of tribological properties of castor oil with various carbonaceous micro- and nano-friction modifiers. J Tribol 139:061802. https://doi.org/10.1115/1.4036379
7. Wang B, Qiu F, Barber GC, Zou Q, Wang J, Guo S, Jiang Q (2022) Role of nano-sized materials as lubricant additives in friction and wear reduction: a review. Wear 204206:490–491. https://doi.org/10.1016/j.wear.2021.204206
8. Zhang Y, Xu S, Zhao Z, Shi J, Zhao Y, Zhang G, Wu Z (2022) Mass-produced Cu nanoparticles as lubricant additives for reducing friction and wear. Lubr Sci 34(4):235–246. https://doi.org/10.1002/ls.1585
9. Uflyand IE, Zhinzhilo VA, Burlakova VE (2019) Metal-containing nanomaterials as lubricant additives: state-of-the-art and future development. Friction 7(2):93–116. https://doi.org/10.1007/s40544-019-0261-y
10. Kulkarni T, Autee A, Toksha B, Chatterjee A, (2022). Data-driven modeling for tribological performance of nano-lubricants using artificial neural network. In *2022 IEEE International Conference on Nanoelectronics, Nanophotonics, Nanomaterials, Nanobioscience & Nanotechnology (5NANO)* (pp. 1–12). Presented at the 2022 IEEE International Conference on Nanoelectronics, Nanophotonics, Nanomaterials, Nanobioscience & Nanotechnology (5NANO). https://doi.org/10.1109/5NANO53044.2022.9828932
11. Kotia A, Rajkhowa P, Rao GS, Ghosh SK (2018) Thermophysical and tribological properties of nanolubricants: a review. Heat Mass Transf 54(11):3493–3508. https://doi.org/10.1007/s00231-018-2351-1
12. Gulzar M, Masjuki HH, Kalam MA, Varman M, Zulkifli NWM, Mufti RA, Zahid R (2016) Tribological performance of nanoparticles as lubricating oil additives. J Nanopart Res 18(8):223. https://doi.org/10.1007/s11051-016-3537-4
13. Liu X, Xu N, Li W, Zhang M, Chen L, Lou W, Wang X (2017) Exploring the effect of nanoparticle size on the tribological properties of SiO2 / polyalkylene glycol nanofluid under different lubrication conditions. Tribol Int 109:467–472. https://doi.org/10.1016/j.triboint.2017.01.007
14. Lahouij I, Vacher B, Martin J-M, Dassenoy F (2012) IF-MoS2 based lubricants: Influence of size, shape and crystal structure. Wear 296(1):558–567. https://doi.org/10.1016/j.wear.2012.07.016
15. Birleanu C, Pustan M, Cioaza M, Molea A, Popa F, Contiu G (2022) Effect of TiO2 nanoparticles on the tribological properties of lubricating oil: an experimental investigation. Sci Rep 12:5201. https://doi.org/10.1038/s41598-022-09245-2
16. Shahnazar S, Bagheri S, Abd Hamid SB (2016) Enhancing lubricant properties by nanoparticle additives. Int J Hydrogen Energy 41(4):3153–3170. https://doi.org/10.1016/j.ijhydene.2015.12.040
17. Chen Y, Renner P, Liang H (2019) Dispersion of nanoparticles in lubricating oil: a critical review. Lubricants 7(1):7. https://doi.org/10.3390/lubricants7010007
18. Kerni L, Raina A, Haq MIU (2019) Friction and wear performance of olive oil containing nanoparticles in boundary and mixed lubrication regimes. Wear 426–427:819–827. https://doi.org/10.1016/j.wear.2019.01.022
19. Jiao D, Zheng S, Wang Y, Guan R, Cao B (2011) The tribology properties of alumina/silica composite nanoparticles as lubricant additives. Appl Surf Sci 257(13):5720–5725. https://doi.org/10.1016/j.apsusc.2011.01.084
20. Luo T, Wei X, Zhao H, Cai G, Zheng X (2014) Tribology properties of Al2O3/TiO2 nanocomposites as lubricant additives. Ceramics Int 40(7 Part A):10103–10109. https://doi.org/10.1016/j.ceramint.2014.03.181
21. Song X, Zheng S, Zhang J, Li W, Chen Q, Cao B (2012) Synthesis of monodispersed ZnAl2O4 nanoparticles and their tribology properties as lubricant additives. Mater Res Bull 47(12):4305–4310. https://doi.org/10.1016/j.materresbull.2012.09.013
22. Wang XL, Yin YL, Zhang GN, Wang WY, Zhao KK (2013) Study on antiwear and repairing performances about mass of nano-copper lubricating additives to 45 steel. Phys Procedia 50:466–472. https://doi.org/10.1016/j.phpro.2013.11.073
23. Zhang C, Zhang S, Yu L, Zhang Z, Wu Z, Zhang P (2012) Preparation and tribological properties of water-soluble copper/silica nanocomposite as a water-based lubricant additive. Appl Surf Sci 259:824–830. https://doi.org/10.1016/j.apsusc.2012.07.132
24. Yu HL, Xu Y, Shi PJ, Wang HM, Zhao Y, Xu BS, Bai ZM (2010) Tribological behaviors of surface-coated serpentine ultrafine powders as lubricant additive. Tribol Int 43(3):667–675. https://doi.org/10.1016/j.triboint.2009.10.006
25. Xie H, Jiang B, Liu B, Wang Q, Xu J, Pan F (2016) An investigation on the tribological performances of the SiO2/MoS2 hybrid nanofluids for magnesium alloy-steel contacts. Nanoscale Res Lett 11(1):329. https://doi.org/10.1186/s11671-016-1546-y
26. Zhang S, Li Y, Hu L, Feng D, Wang H (2017) Antiwear effect of Mo and W nanoparticles as additives for multialkylated cyclopentanes oil in vacuum. J Tribol 139(2):021607. https://doi.org/10.1115/1.4033638
27. Singh Y, Chaudhary V, Pal V (2020) Friction and wear characteristics of the castor oil with TiO2 as an additives. Mat Today: Proc 26:2972–2976. https://doi.org/10.1016/j.matpr.2020.02.612
28. Luo T, Wei X, Huang X, Huang L, Yang F (2014) Tribological properties of Al2O3 nanoparticles as lubricating oil additives. Ceram Int 40(5):7143–7149. https://doi.org/10.1016/j.ceramint.2013.12.050

29. Gu K, Chen B, Chen Y (2013) Preparation and tribological properties of lanthanum-doped TiO2 nanoparticles in rapeseed oil. J Rare Earths 31(6):589–594. https://doi.org/10.1016/S1002-0721(12)60325-1
30. Ye W, Cheng T, Ye Q, Guo X, Zhang Z, Dang H (2003) Preparation and tribological properties of tetrafluorobenzoic acid-modified TiO2 nanoparticles as lubricant additives. Mater Sci Eng, A 359(1):82–85. https://doi.org/10.1016/S0921-5093(03)00353-8
31. Laad M, Jatti VKS (2018) Titanium oxide nanoparticles as additives in engine oil. J King Saud Univ - Eng Sci 30(2):116–122. https://doi.org/10.1016/j.jksues.2016.01.008
32. Nunn N, Mahbooba Z, Ivanov MG, Ivanov DM, Brenner DW, Shenderova O (2015) Tribological properties of polyalphaolefin oil modified with nanocarbon additives. Diam Relat Mater 54:97–102. https://doi.org/10.1016/j.diamond.2014.09.003
33. Ali MKA, Hou X, Abdelkareem MAA (2020) Anti-wear properties evaluation of frictional sliding interfaces in automobile engines lubricated by copper/graphene nanolubricants. Friction 8(5):905–916. https://doi.org/10.1007/s40544-019-0308-0
34. Ali MKA, Xianjun H, Mai L, Qingping C, Turkson RF, Bicheng C (2016) Improving the tribological characteristics of piston ring assembly in automotive engines using Al2O3 and TiO2 nanomaterials as nano-lubricant additives. Tribol Int 103:540–554. https://doi.org/10.1016/j.triboint.2016.08.011
35. Kumar Chaurasia S, Kumar Singh N, Kumar Singh L (2020) Friction and wear behavior of chemically modified Sal (Shorea Robusta) oil for bio based lubricant application with effect of CuO nanoparticles. Fuel 282:118762. https://doi.org/10.1016/j.fuel.2020.118762
36. Singh Y, Rahim EA, Singh NK, Sharma A, Singla A, Palamanit A (2022) Friction and wear characteristics of chemically modified mahua (madhuca indica) oil based lubricant with SiO2 nanoparticles as additives. Wear 508–509:204463. https://doi.org/10.1016/j.wear.2022.204463
37. Nagarajan T, Khalid M, Sridewi N, Jagadish P, Shahabuddin S, Muthoosamy K, Walvekar R (2022) Tribological, oxidation and thermal conductivity studies of microwave synthesised molybdenum disulfide (MoS2) nanoparticles as nano-additives in diesel based engine oil. Sci Rep 12(1):14108. https://doi.org/10.1038/s41598-022-16026-4
38. Guo D, Xie G, Luo J (2013) Mechanical properties of nanoparticles: basics and applications. J Phys D Appl Phys 47(1):013001
39. Akl S, Elsoudy S, Abdel-Rehim AA, Salem S, Ellis M (2021) Recent advances in preparation and testing methods of engine-based nanolubricants: a state-of-the-art review. Lubricants 9(9):85. https://doi.org/10.3390/lubricants9090085
40. Deepika. (2020) Nanotechnology implications for high performance lubricants. SN Applied Sci 2(6):1128. https://doi.org/10.1007/s42452-020-2916-8
41. Hou X, He J, Yu L, Li Z, Zhang Z, Zhang P (2014) Preparation and tribological properties of fluorosilane surface-modified lanthanum trifluoride nanoparticles as additive of fluoro silicone oil. Appl Surf Sci 316:515–523. https://doi.org/10.1016/j.apsusc.2014.07.171
42. Wang C, Zhang X, Jia W, Deng Q, Leng Y (2019) Preparation and tribological properties of modified field's alloy nanoparticles as additives in liquid poly-alfa-olefin solution. J Tribol 141:052001. https://doi.org/10.1115/1.4042768
43. Kumar H, Harsha AP (2020) Investigation on friction, anti-wear, and extreme pressure properties of different grades of polyalphaolefins with functionalized multi-walled carbon nanotubes as an additive. J Tribol 142:081702. https://doi.org/10.1115/1.4046571
44. Allawzi M, Abu-Arabi MK, Al-zoubi HS, Tamimi A (1998) Physicochemical characteristics and thermal stability of Jordanian jojoba oil. J Am Oil Chem' Soc 75(1):57–62. https://doi.org/10.1007/s11746-998-0010-2
45. Toksha BG, Shirsath SE, Patange SM, Jadhav KM (2008) Structural investigations and magnetic properties of cobalt ferrite nanoparticles prepared by sol–gel auto combustion method. Solid State Commun 147(11):479–483. https://doi.org/10.1016/j.ssc.2008.06.040
46. Jadhav SS, Shirsath SE, Toksha BG, Patange SM, Shengule DR, Jadhav KM (2010) Structural and electric properties of zinc substituted NiFe2O4 nanoparticles prepared by co-precipitation method. Physica B 405(12):2610–2614. https://doi.org/10.1016/j.physb.2010.03.008
47. Tonde S, More S, Hazra C, Kundu D, Joshi S, Satdive A, Chatterjee A (2022) 1D sub 10 nm nanofabrication of ultrahydrophobic Ag@TiO2 nanowires and their photocatalytic, UV shielding and antibacterial properties. Adv Powder Technol 33(2):103404. https://doi.org/10.1016/j.apt.2021.103404
48. Hachem K, Ansari MJ, Saleh RO, Kzar HH, Al-Gazally ME, Altimari US, Kianfar E (2022) Methods of chemical synthesis in the synthesis of nanomaterial and nanoparticles by the chemical deposition method: a review. BioNanoScience 12(3):1032–1057. https://doi.org/10.1007/s12668-022-00996-w
49. Gan YX, Jayatissa AH, Yu Z, Chen X, Li M (2020) Hydrothermal synthesis of nanomaterials. J Nanomater 2020:e8917013. https://doi.org/10.1155/2020/8917013
50. Jamkhande PG, Ghule NW, Bamer AH, Kalaskar MG (2019) Metal nanoparticles synthesis: an overview on methods of preparation, advantages and disadvantages, and applications. J Drug Deliver Sci Technol 53:101174. https://doi.org/10.1016/j.jddst.2019.101174
51. Abid N, Khan AM, Shujait S, Chaudhary K, Ikram M, Imran M, Maqbool M (2022) Synthesis of nanomaterials using various top-down and bottom-up approaches, influencing factors, advantages, and disadvantages: a review. Adv Colloid Interface Sci 300:102597. https://doi.org/10.1016/j.cis.2021.102597
52. Chang Q, Liang H, Shi B, Li X, Zhang Y, Zhang L, Wu H (2021) Ethylenediamine-assisted hydrothermal synthesis of NiCo2O4 absorber with controlled morphology and excellent absorbing performance. J Colloid Interface Sci 588:336–345. https://doi.org/10.1016/j.jcis.2020.12.099
53. Li Z, Zhong W, Gao D, Chen F, Yu H (2023) CdIn2S4-xSex solid-solution nanocrystal photocatalyst: one-step hydrothermal synthesis, controllable band structure, and improved H2-evolution activity. Adv Sustain Syst 7(1):2200030. https://doi.org/10.1002/adsu.202200030
54. Kulkarni T, Toksha B, Chatterjee A, Naik J, Autee A (2023) Anti-wear (AW) and extreme-pressure (EP) behavior of jojoba oil dispersed with green additive CaCO3 nanoparticles. J Eng Appl Sci 70(1):29. https://doi.org/10.1186/s44147-023-00202-y

55. Márquez-Martínez P, Martínez-Franco E, Cuenca-Alvarez R, Hurtado-Macías A, García-Moreno AI, Alvarado-Orozco JM, Ruiz-Luna H (2022) Processing and characterization of Inconel 718/Al2O3 nanocomposite powder fabricated by different techniques. Powder Technol 398:117124. https://doi.org/10.1016/j.powtec.2022.117124
56. Wanatasanapan VV, Abdullah MZ, Gunnasegaran P (2020) Effect of TiO2-Al2O3 nanoparticle mixing ratio on the thermal conductivity, rheological properties, and dynamic viscosity of water-based hybrid nanofluid. J Market Res 9(6):13781–13792. https://doi.org/10.1016/j.jmrt.2020.09.127
57. Santos EP, Dutra AJB, Oliveira JF (2015) The effect of jojoba oil on the surface properties of calcite and apatite aiming at their selective flotation. Int J Miner Process 143:34–38. https://doi.org/10.1016/j.minpro.2015.08.002
58. Umar S, Sulaiman F, Abdullah N, Mohamad SN (2018) Investigation of the effect of pH adjustment on the stability of nanofluid. AIP Conf Proc 2031(1):020031. https://doi.org/10.1063/1.5066987
59. Ali ARI, Salam B (2020) A review on nanofluid: preparation, stability, thermophysical properties, heat transfer characteristics and application. SN Appl Sci 2(10):1636. https://doi.org/10.1007/s42452-020-03427-1
60. Badmus SO, Amusa HK, Oyehan TA, Saleh TA (2021) Environmental risks and toxicity of surfactants: overview of analysis, assessment, and remediation techniques. Environ Sci Pollut Res 28(44):62085–62104. https://doi.org/10.1007/s11356-021-16483-w
61. Kawashima S, Seo J-WT, Corr D, Hersam MC, Shah SP (2014) Dispersion of CaCO3 nanoparticles by sonication and surfactant treatment for application in fly ash–cement systems. Mater Struct 47(6):1011–1023. https://doi.org/10.1617/s11527-013-0110-9
62. de Oliveira LG, de Paiva AP, Balestrassi PP, Ferreira JR, da Costa SC, da Silva Campos PH (2019) Response surface methodology for advanced manufacturing technology optimization: theoretical fundamentals, practical guidelines, and survey literature review. Int J Adv Manufact Technol 104(5):1785–1837. https://doi.org/10.1007/s00170-019-03809-9
63. Ahmed Ali MK, Xianjun H, Essa FA, Abdelkareem MAA, Elagouz A, Sharshir SW (2018) Friction and wear reduction mechanisms of the reciprocating contact interfaces using nanolubricant under different loads and speeds. J Tribol 140:051606. https://doi.org/10.1115/1.4039720
64. Chen Y, Wang X, Han Z, Sinyukov A, Clearfield A, Liang H (2022) Amphiphilic zirconium phosphate nanoparticles as tribo-catalytic additives of multi-performance lubricants. J Tribol 144:071901. https://doi.org/10.1115/1.4053352
65. Lei W, Tang W, Mo X, Tian Z, Shen P, Ouyang T (2023) Tribological evaluation of few-layer nitrogen-doped graphene as an efficient lubricant additive on engine cylinder liner: experiment and mechanism investigation. J Tribol 145:062201. https://doi.org/10.1115/1.4056905
66. Jason YJJ, How HG, Teoh YH, Chuah HG (2020) A study on the tribological performance of nanolubricants. Processes 8(11):1372. https://doi.org/10.3390/pr8111372
67. Dai W, Kheireddin B, Gao H, Liang H (2016) Roles of nanoparticles in oil lubrication. Tribol Int 102:88–98. https://doi.org/10.1016/j.triboint.2016.05.020
68. Yadgarov L, Petrone V, Rosentsveig R, Feldman Y, Tenne R, Senatore A (2013) Tribological studies of rhenium doped fullerene-like MoS2 nanoparticles in boundary, mixed and elasto-hydrodynamic lubrication conditions. Wear 297(1):1103–1110. https://doi.org/10.1016/j.wear.2012.11.084
69. Wu H, Zhao J, Xia W, Cheng X, He A, Yun JH, Jiang Z (2017) A study of the tribological behaviour of TiO2 nano-additive water-based lubricants. Tribol Int 109:398–408. https://doi.org/10.1016/j.triboint.2017.01.013
70. Ingole S, Charanpahari A, Kakade A, Umare SS, Bhatt DV, Menghani J (2013) Tribological behavior of nano TiO2 as an additive in base oil. Wear 301(1):776–785. https://doi.org/10.1016/j.wear.2013.01.037
71. Chen Y, Yang K, Lin H, Zhang F, Xiong B, Zhang H, Zhang C (2022) Important contributions of multidimensional nanoadditives on the tribofilms: from formation mechanism to tribological behaviors. Compos B Eng 234:109732. https://doi.org/10.1016/j.compositesb.2022.109732
72. Qi J, Guan D, Nutter J, Wang B, Rainforth WM (2022) Insights into tribofilm formation on Ti-6V-4Al in a bioactive environment: correlation between surface modification and micro-mechanical properties. Acta Biomater 141:466–480. https://doi.org/10.1016/j.actbio.2022.01.027
73. Liu G, Li G, Zhao F, Myshkin NK, Zhang G (2021) Role of tribochemistry reactions of B4C on tribofilm growth at a PEEK–steel interface in simulated body fluids. RSC Adv 11(52):32717–32729. https://doi.org/10.1039/D1RA05447C
74. Haas KL, Franz KJ (2009) Application of metal coordination chemistry to explore and manipulate cell biology. Chem Rev 109(10):4921–4960. https://doi.org/10.1021/cr900134a
75. Wu Y, Sun T, He Z, Zeng X, Ren T, de Vries E, van der Heide E (2021) Study on the relationship between the tribological properties and oxidation degree of graphene derivatives in O/W emulsion. Tribol Int 157:106875. https://doi.org/10.1016/j.triboint.2021.106875
76. Ueda M, Kadiric A, Spikes H (2021) Influence of steel surface composition on ZDDP tribofilm growth using ion implantation. Tribol Lett 69(2):62. https://doi.org/10.1007/s11249-021-01436-8

Publisher's Note